Adaptive Power Compensation Based Frequency Regulation Strategy of Wind Turbine System

Hongqing Liu, Xiaokang Liu, *Member, IEEE,* Liansong Xiong, *Senior Member, IEEE,* Mingxian Li, and Yixin Zhu

***Abstract*—Given the increasing penetration of wind power generation, the power system faces great challenges in frequency regulation due to reduction in system inertia. This paper proposes an adaptive power compensation based frequency regulation (FR) strategy of the wind turbine system (WTS). In a frequency transient event, the proposed strategy exploits power excitation method to estimate the disturbance level, which enables the WTS to timely and accurately participate in FR. After the system frequency and the rate of change of frequency meet their requirements, the droop control is adopted to smooth the WTS out of the FR mode and further improve the frequency quality. By analyzing the operation mode and determining the switching logic, detailed implementation of the proposed strategy is developed. Its excellent frequency response performance is verified via results of hardware-in-the-loop experiment and MATLAB/Simulink-based simulation.**

***Index Terms*—Adaptive power compensation, frequency regulation, disturbance estimation, power excitation method, wind turbine system.**

I. Introduction

THE wind turbine system (WTS), which is interfaced with the grid through power converters to decouple the rotational kinetic energy from the system, cannot provide necessary inertia or damping to the grid. Accordingly, the continuously increasing share of WTS has been weakening the power system inertia [1]–[3], reducing system robustness against power disturbances and causing great challenges to the safe and stable operation of power grid [4]. In the context of bulk wind power penetration, grid-friendly frequency regulation (FR) control of WTS plays an important role, if frequency response characteristics of its integrated network need to be improved [5], [6].

Numerous grid codes across the globe focusing on wind power generation have clearly stipulated that the WTS needs to participate in FR [7]–[9]. This generally requires the WTS to make use of either virtual inertia control (VIC) or temporary over-production (TOP) control [10]. The former one uses a frequency coupling control loop to release kinetic energy stored in the WTS rotor and achieve power balance [11]. During its implementation, the frequency deviation and the rate of change of frequency (RoCoF) are considered simultaneously (known as the integrated control) [11], [12]. However, the VIC has certain limitations for FR, encompassing difficulty in control parameters design [13], [14] and insufficient use of capacity. Indeed, the FR performance of VIC is affected by the comprehensive effect of control parameters, disturbance, and system parameters; due to the randomness of disturbance, it is hard to choose appropriate control parameters that provide highly-reliable FR performance [15]. Besides, in the early stage of disturbance, the supporting power for grid frequency is less than the maximum allowable value, failing to make full use of the FR potential of the WTS [16].

Compared with the VIC, the TOP control is based on the system information of over-production capacity and makes the greatest possible contribution under any operating conditions. It dispenses with the need for complex parameter tuning [10], and releases more energy in a short time; owing to quicker compensation of imbalance power, the frequency nadir and RoCoF indicators can be improved. Besides, the TOP control can completely suppress the subsequent frequency oscillations and overshoots [17]. Analogous to the TOP control, the rapid power compensation (RPC) strategy proposed in [18] fully utilizes the idle capacity of grid-tied converter and quickly compensates the imbalance power of grid. Though the aforementioned TOP and RPC control strategies exhaust the idle energy reserve of WTS for FR support, it is difficult to decide their initial output due to randomness and uncertainty of the disturbance. If the maximum FR power allowed by the WTS is directly used as the supporting power, a reverse disturbance to the system power can be caused when the applied FR power dominates over the initial disturbance, introducing secondary frequency transient and deteriorating system stability.

To effectively provide inertial support and improve the frequency response performance, an adaptive power compensation (APC) control strategy is proposed in this manuscript. In the case of frequency deterioration caused by system disturbance, the power excitation method is first used to estimate the disturbance. Subsequently, the WTS quickly releases the rotational kinetic energy and outputs FR power in response to the disturbance, avoiding the blindness of TOP/RPC control to unconditionally inject the maximum FR power. When the frequency deviation and RoCoF meet the regulatory requirements, the APC switches to droop control and assures smooth exit of WTS from FR participation, avoiding long-term FR

Manuscript received July 22, 2021; revised November 26, 2021. The work was supported by the National Natural Science Foundation of China (51807079). *(Corresponding author: Xiaokang Liu.)*

Hongqing Liu is with the School of Electrical and Power Engineering, China University of Mining and Technology, Xuzhou 221000, China, e-mail:liuhq@cumt.edu.cn.

Xiaokang Liu is with the Department of Electronics, Information and Bioengineering, Politecnico di Milano, 20133 Milan, Italy, e-mail: xiaokang.liu@polimi.it.

Liansong Xiong is with the School of Automation, Nanjing Institute of Technology, Nanjing 211167, China, e-mail: xiongliansong@163.com.

Mingxian Li is with StateGrid Jiaxing Power Supply Company, Jiaxing 314001, China, e-mail: mingxian.li@foxmail.com.

Yixin Zhu is with the School of IoT engineering, Jiangnan University, Wuxi 214122, China, e-mail: zhuyixin1987@163.com.

support from WTS and subsequent frequency disturbances triggered by the termination of FR.

II. Frequency Response and Challenges of WTS

A. Frequency Response of Grid-tied WTS

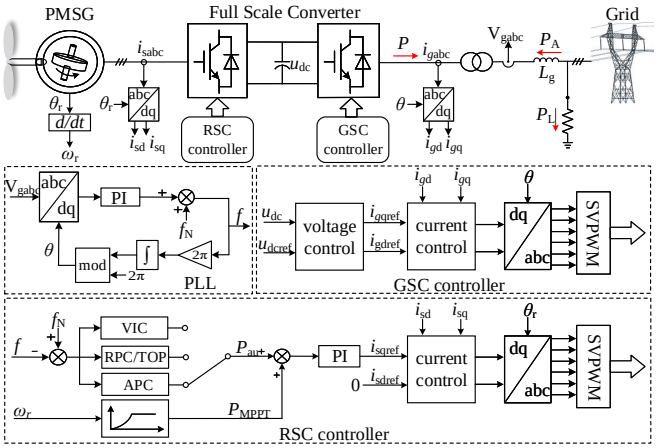

Fig. 1. Block diagram of a single grid-tied WTS.

Fig. 1 shows the block diagram of a single grid-tied WTS, where RSC (GSC) represents the rotor (grid)-side converter. For multiple wind generators in the power grid and the same wind speed in the wind farm, the grid can be simplified by regarding the generators as equivalent single units without considering the internal FR power distribution. By only considering the inertial response of the synchronous generator set, and neglecting the primary and secondary frequency regulation actions, the dynamic response of system frequency can be obtained by the rotor motion equation of equivalent generator. Namely, the system frequency is determined jointly by the output power of WTS and the absorbed power of grid, as [19]

$$T_{\mathrm{J}}\frac{df}{dt}=P-P_{\mathrm{A}} \tag{1}$$

where, T_{J} is the equivalent inertia coefficient, f is the system frequency, P is the electromagnetic power output by WTS, and P_{A} is the power absorbed at the grid side.

For better utilization of wind energy, the WTS operates at the maximum power point tracking (MPPT) mode, and

$$P=P_{\mathrm{MPPT}}=k_{\max}{\omega_{\mathrm{r}}}^{3} \tag{2}$$

where, ω_{r} is the rotor angular speed of WTS, $k_{\max}$ is the maximum output coefficient of WTS, and P_{MPPT} is the WTS output power under the MPPT control.

After a power disturbance of grid, the WTS outputs auxiliary power to participate in the FR. Its total output power P is composed of the MPPT power before disturbance, P_{MPPT0} (considering the MPPT power remains unchanged in the early stage of disturbance, [20]), and the auxiliary FR power, P_{au}, i.e.,

$$P=P_{\mathrm{MPPT0}}+P_{\mathrm{au}} \tag{3}$$

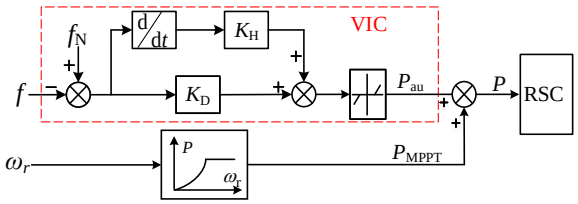

Fig. 2. Integrated control diagram for WTS incorporating VIC.

The absorbed power by GSC, P_{A}, consists of the steady-state load power P_{L0}, load disturbance power ΔP_{L}, and the load frequency response, yielding

$$P_{\mathrm{A}}=P_{\mathrm{L0}}+\Delta P_{\mathrm{L}}-D_{\mathrm{L}}\left(f_{\mathrm{N}}-f\right) \tag{4}$$

where D_{L} is the equivalent damping coefficient of load. By combining (1), (2), (3), and (4), the frequency response of system can be described by

$$T_{\mathrm{J}}\frac{df}{dt}=P_{\mathrm{MPPT0}}+P_{\mathrm{au}}-P_{\mathrm{L0}}-\Delta P_{\mathrm{L}}+D_{\mathrm{L}}\left(f_{\mathrm{N}}-f\right) \tag{5}$$

By considering $P_{\mathrm{MPPT0}}=P_{\mathrm{L0}}$, (5) can be rewritten as

$$T_{\mathrm{J}}\frac{df}{dt}=P_{\mathrm{au}}-\Delta P_{\mathrm{L}}+D_{\mathrm{L}}\left(f_{\mathrm{N}}-f\right) \tag{6}$$

Solution to (6) gives Δf and RoCoF of the system as

$$\Delta f=f_{\mathrm{N}}-f=\frac{\Delta P_{\mathrm{L}}-P_{\mathrm{au}}}{D_{\mathrm{L}}}\left(1-e^{-\frac{D_{\mathrm{L}}}{T_{\mathrm{J}}}t}\right) \tag{7}$$

$$R=\frac{df}{dt}=\frac{\Delta P_{\mathrm{L}}-P_{\mathrm{au}}}{T_{\mathrm{J}}}e^{-\frac{D_{\mathrm{L}}}{T_{\mathrm{J}}}t} \tag{8}$$

The initial moment after power disturbance is usually associated with the maximum active power imbalance, so the pertinent RoCoF is the largest. On the contrary, the maximum value of Δf appears at steady state. Therefore,

$$\begin{cases}\Delta f|_{\max}=\lim\limits_{t\to\infty}\left(f_{\mathrm{N}}-f\right)=\dfrac{\Delta P_{\mathrm{L}}-P_{\mathrm{au}}}{D_{\mathrm{L}}}\\ \mathrm{RoCoF}|_{\max}=\lim\limits_{t\to 0}\dfrac{\mathrm{d}f}{\mathrm{d}t}=\dfrac{\Delta P_{\mathrm{L}}-P_{\mathrm{au}}}{T_{\mathrm{J}}}\end{cases} \tag{9}$$

It can be seen from (9) that the maximum RoCoF is proportional to the system imbalance power and inversely proportional to the system inertia. The maximum Δf is inversely proportional to load damping and independent of system inertia. If the WTS does not participate in FR, P_{au} equals 0, and Δf and RoCoF are likely to exceed the limits for frequency-related protection, especially in a system with low inertia and weak damping. To assure system frequency stability and optimize the frequency nadir and RoCoF, P_{au} should be as close as possible to ΔP_{L}, thereby reducing the system imbalance power and avoiding a series of frequency-related problems.

B. Challenges of Conventional FR Control Strategy

With reference to the control diagram in Fig. 2, the VIC combines inertia control with droop control to release the

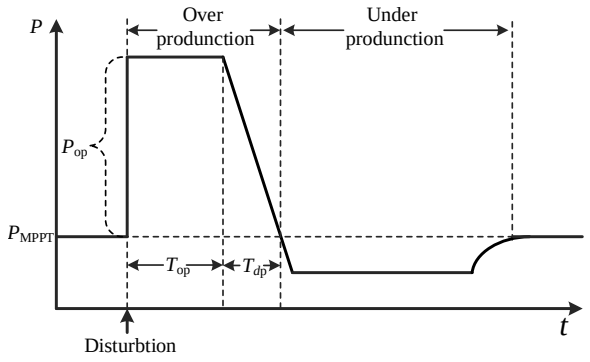

Fig. 3. Power released by WTS using TOP control.

rotational kinetic energy reserved in the WTS. The FR power generated by this integrated control is

$$P_{\mathrm{au}} = K_{\mathrm{H}} \frac{d(f_{\mathrm{N}} - f)}{dt} + K_{\mathrm{D}}(f_{\mathrm{N}} - f) \tag{10}$$

where K_{H} and K_{D} are the gains of inertia and droop control, respectively.

Combining (6), (7), (8), (9), and (10), we can get

$$\begin{cases} \Delta f|_{\max} = \lim\limits_{t\to\infty} (f_{\mathrm{N}} - f) = \dfrac{\Delta P_{\mathrm{L}}}{K_{\mathrm{D}} + D_L} \\ \mathrm{RoCoF}|_{\max} = \lim\limits_{t\to 0} \dfrac{\mathrm{d}\Delta f}{\mathrm{d}t} = \dfrac{\Delta P_{\mathrm{L}}}{K_{\mathrm{H}} + T_{\mathrm{J}}} \end{cases} \tag{11}$$

To minimize Δf and RoCoF in (11), K_{D} and K_{H} need to be optimized according to several parameters of the system, encompassing D_{L}, T_{J}, and ΔP_{L}. However, these parameters are difficult to detect in advance and change with the system operation mode, load fluctuations, and line faults [21]. Generally, for the best stability of grid frequency after disturbance, the VIC parameter design takes into account the maximum load disturbance and the lowest values of inertia and damping. However, this consideration fails to achieve the optimal FR. Besides, the FR power released by WTS with VIC strategy changes with frequency, i.e., the inertia potential of WTS cannot be fully utilized.

Compared with the VIC that slowly participates in FR based on Δf and RoCoF, the TOP (see Fig. 3 for illustration of its released power) and RPC strategies achieve fast compensation of the imbalance power by exploiting the complete FR potential of WTS. At the moment of disturbance, constant FR power (P_{op} in Fig. 3) decoupled from the system frequency is released for grid support, avoiding the use of grid parameters as with the VIC. By considering the FR auxiliary power to be $P_{\mathrm{au}} = P_{\mathrm{op}}$ when adopting RPC/TOP control, (9) can be reformulated as

$$\begin{cases} \Delta f|_{\max} = \dfrac{\Delta P_{\mathrm{L}} - P_{\mathrm{op}}}{D_L} \\ \mathrm{RoCoF}|_{\max} = \dfrac{\Delta P_{\mathrm{L}} - P_{\mathrm{op}}}{T_{\mathrm{J}}} \end{cases} \tag{12}$$

The optimal frequency indexes of system, during the inertia response stage, require the FR power from WTS P_{op} equal to ΔP_{L}, such that the system power imbalance is reduced to the minimum. However, this is difficult to achieve due to the randomness of disturbance, and the pertinent consequences are analyzed in the following.

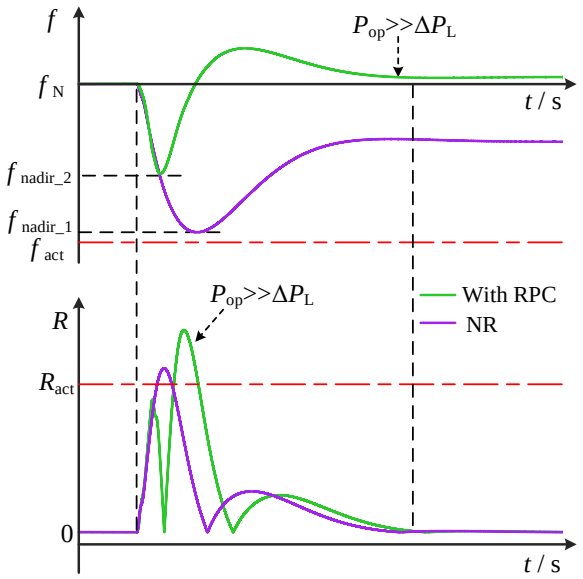

Fig. 4. Frequency response of TOP/RPC control-based WTS, when $P_{\mathrm{op}} \gg \Delta P_{\mathrm{L}}$. NR: natural response of the frequency.

After occurrence of a small disturbance in the system, if $P_{\mathrm{op}} \gg \Delta P_{\mathrm{L}}$, the initial output dominates over the power shortage caused by disturbance (see Fig. 4). Excessive WTS participation in FR will cause reverse system frequency deviation and severe secondary disturbance of RoCoF, which can trigger frequency-related protections when their thresholds (f_{act} and R_{act} in Fig. 4) are reached. At the same time, economy of grid-connected WTS power generation is reduced. Conversely, if the random system disturbance dominates over the provided FR power, i.e., $P_{\mathrm{op}} \ll \Delta P_{\mathrm{L}}$, frequency indexes of system will directly exceed their limits. Therefore, providing FR power that follows the estimated disturbance is the key to achieving high-quality FR. To this end, the disturbance level must be reasonably evaluated, with its error limited within an allowable range.

III. System Disturbance Estimation

As previously discussed, power fluctuations of the system can be critical for the safety, stability, and control of frequency. The system imbalance power, which is introduced by a random disturbance and causes frequency fluctuation, depends on the inertia and damping of system. The grid inertia reflects the ability of system to suppress frequency changes, and can be viewed as constant for a short time after the system disturbance (likewise for system damping). On this basis, system inertia and damping parameters can be assessed by measurement of f and RoCoF at different times, along with proper injection of a testing excitation into the system. Then, the disturbance power can be estimated jointly by the short term frequency response, and inertia and damping parameters. This procedure is detailed as follows.

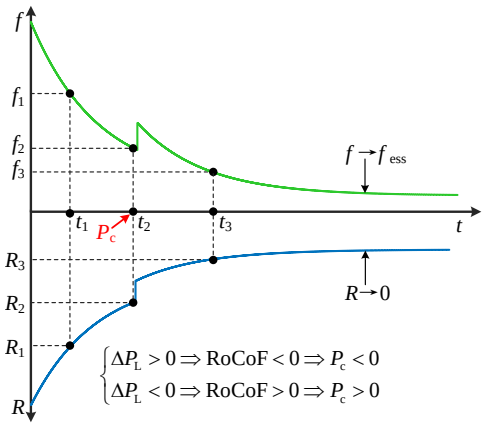

Fig. 5. Illustration of critical timing and system frequency dynamics with the power excitation method. f_{ess} is the steady-state frequency with energy storage system applied. Sudden load power increase ($\Delta P_{\text{L}} > 0$) is assumed.

At the moment of disturbance, if the WTS does not participate in system FR (i.e., $P_{\text{au}} = 0$), (6) is rewritten as

$$T_{\text{J}} \frac{df}{dt} = -\Delta P_{\text{L}} + D_{\text{L}} \left(f_{\text{N}} - f\right) \tag{13}$$

From (13), the system disturbance can be obtained as

$$\Delta P_{\text{L}} = D_{\text{L}} \left(f_{\text{N}} - f\right) - T_{\text{J}} \frac{df}{dt} \tag{14}$$

From (14), when measurement results of f and df/dt (i.e. RoCoF) caused by disturbance are available, the system inertia and damping are pre-requisites for obtaining the disturbance power. However, due to the high penetration level of new energy generation and complexity of inertia structure, the equivalent inertia/damping of system has prominent time-varying characteristics that cannot be determined in advance.

In this paper, the power excitation method is used to obtain the real-time system inertia and damping. With reference to Fig. 5, a positive power disturbance ($\Delta P_{\text{L}} > 0$) causes the frequency to drop with time. When Δf (or RoCoF) reaches the predefined threshold at t_1, the frequency dynamics yield

$$T_{\text{J}} \left.\frac{df}{dt}\right|_{t=t_1} = -\Delta P_{\text{L}} + D_{\text{L}} \left(f_{\text{N}} - f_1\right) \tag{15}$$

where f_1 and R_1 ($R = df/dt$ represents the RoCoF hereafter) are obtained by frequency sampling and recording at t_1.

At time t_2 ($t_2 > t_1$), the system frequency response is

$$T_{\text{J}} \left.\frac{df}{dt}\right|_{t=t_2} = -\Delta P_{\text{L}} + D_{\text{L}} \left(f_{\text{N}} - f_2\right) \tag{16}$$

Similarly, f_2 and R_2 are obtain at t_2; at the same time, a testing excitation P_{c} is applied (see Fig. 5). The direction of P_{c} coincides with that of RoCoF and opposes to that of disturbance, thus avoiding further deterioration of system frequency response. When the system is subject to a positive disturbance, the system frequency decreases, in which case a reverse P_{c} is applied, and vice versa.

At time t_3 ($t_3 > t_2$), f_3 and R_3 are obtained, and

$$T_{\text{J}} \left.\frac{df}{dt}\right|_{t=t_3} = -\left(\Delta P_{\text{L}} + P_{\text{c}}\right) + D_{\text{L}} \left(f_{\text{N}} - f_3\right) \tag{17}$$

It is worth mentioning that in practice, t and R values are calculated as average sample values in three time windows, t_1, t_2, and t_3, yielding

$$\begin{cases} f_{\text{m}} = \dfrac{1}{N} \displaystyle\sum_{k=1}^{N} f_{mk} \\ R_{\text{m}} = \dfrac{1}{N} \displaystyle\sum_{k=1}^{N} R_{mk} \end{cases} \tag{18}$$

where, N represents the number of samples in a window, and $m = 1, 2, 3$.

Combining (15), (16), and (17), the system inertia and damping parameters can be obtained as

$$D_{\text{L}} = -\frac{P_{\text{c}} \left(R_2 - R_1\right)}{\left(f_3 - f_2\right)\left(R_2 - R_1\right) - \left(f_2 - f_1\right)\left(R_3 - R_2\right)} \tag{19}$$

$$T_{\text{J}} = \frac{P_{\text{c}} \left(f_2 - f_1\right)}{\left(f_3 - f_2\right)\left(R_2 - R_1\right) - \left(f_2 - f_1\right)\left(R_3 - R_2\right)} \tag{20}$$

Afterward, by combining (14), (18), and (19), the system disturbance power is estimated as

$$P_{\text{L}}^{\text{es}} = \frac{P_{\text{c}} \left[R_1 \left(f_{\text{N}} - f_2\right) - R_2 \left(f_{\text{N}} - f_1\right)\right]}{\left(f_3 - f_2\right)\left(R_2 - R_1\right) - \left(f_2 - f_1\right)\left(R_3 - R_2\right)} \tag{21}$$

By considering the direction of ΔP_{L}, (21) is generalized as

$$P_{\text{L}}^{\text{es}} = \frac{P_{\text{c}} \left[R_1 \left(f_{\text{N}} - f_2\right) - R_2 \left(f_{\text{N}} - f_1\right)\right]}{\left(f_3 - f_2\right)\left(R_2 - R_1\right) - \left(f_2 - f_1\right)\left(R_3 - R_2\right)} \text{sign}\left(R\right) \tag{22}$$

where, $\text{sign}\left(R\right) = \begin{cases} 1 & R > 0 \\ -1 & R < 0 \end{cases}$.

Based on the system disturbance estimation given by (22), the fast FR service can be carried out, by matching the initial FR power to the disturbance power.

IV. Proposed APC Control Strategy

In this paper, an adaptive control is realized by incorporating the disturbance estimation. Various stages and pertinent FR power output with the proposed control are first identified in the case of a large disturbance (see Fig. 6), namely

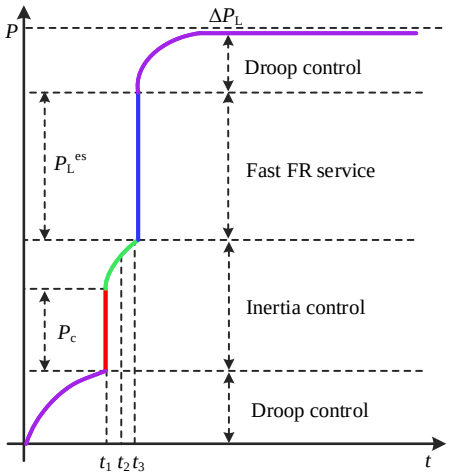

Fig. 6. FR power output by WTS and control stages under the proposed APC control. Sudden load power increase ($\Delta P_{\text{L}} > 0$) is assumed.

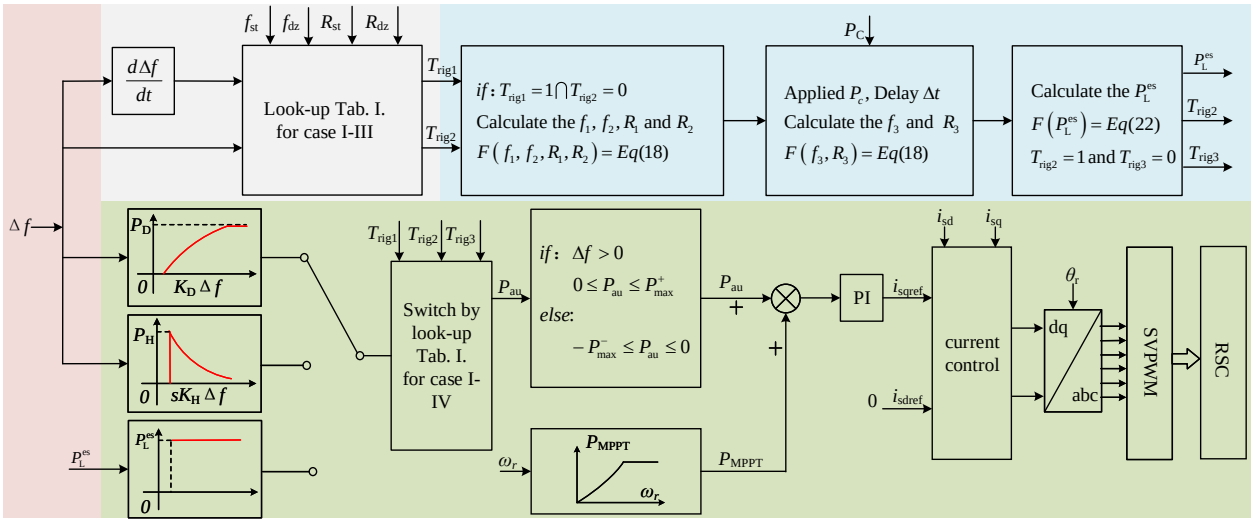

Fig. 7. Detailed implementation of the proposed APC strategy.

1) *Initial droop control*: The WTS previously operates with no FR power output ($t < 0$). After the disturbance, and when Δf and RoCoF are both insignificant ($0 < t < t_1$), the system operates at droop control mode.
2) *Inertia control with disturbance estimation*: When Δf (or RoCoF) reaches a certain threshold at t_1, disturbance estimation starts with a testing power (P_c) injection. Inertia control is used until the end of estimation. Due to the large system RoCoF at the initial stage of frequency response, the inertia control quickly responds to system frequency dynamics and avoids its fast deterioration.
3) *Fast FR service*: After the estimation of disturbance power P_L^{es}, its value is used as the reference for FR power of WTS. This fast FR service provided by WTS effectively suppresses the unbalanced power, and quickly improves the system frequency indexes.
4) *Final droop control*: Reasonable exit time and method of FR are particularly important. Once frequency indexes meet the grid code requirements, the system frequency response is dominated by Δf, which is directly related to the droop control. Therefore, in the later stage of frequency response, the fast FR service is switched to droop control to achieve the smooth exit of FR. Power quality is improved by further reduction of Δf and RoCoF, yet avoiding the frequency second dip caused by improper FR of the WTS. Otherwise, after a long time of deep participation in FR, the frequency will drop again during the recovery of WTS speed, due to the limited rotational inertia of WTS.

To implement the APC strategy, the system operation is divided into four cases (see Table I) according to Δf and RoCoF. Several frequency/RoCoF parameters are used for case selection, including 1) $f_{\rm dz}$ and $R_{\rm dz}$, which are dead-zone thresholds of Δf and RoCoF, respectively; 2) $f_{\rm st}$ and $R_{\rm st}$, which are thresholds for APC operation, and 3) $f_{\rm act}$ and $R_{\rm act}$, which are thresholds to trigger frequency-related protections. Three flag signals ($T_{{\rm rig}m}, m = 1, 2, 3$) are used for the switching logic. The four cases are elaborated as follows:

TABLE I
CASES FOR APC STRATEGY IMPLEMENTATION.

Case	Condition	$T_{\rm rig1}$	$T_{\rm rig2}$	$T_{\rm rig3}$	Power output
I	$\Delta f < f_{\rm dz}$ and $R < R_{\rm dz}$	0	0	1	0
II	$f_{\rm dz} < \lvert\Delta f\rvert < f_{\rm st}$ and $R_{\rm dz} < \lvert R\rvert < R_{\rm st}$	0	0	0	$K_{\rm D}\Delta f$
III	$f_{\rm st} < \lvert\Delta f\rvert < f_{\rm act}$ or $R_{\rm st} < \lvert R\rvert < R_{\rm act}$	1	0	0	$sK_{\rm H}\Delta f$
IV	$f_{\rm st} < \lvert\Delta f\rvert < f_{\rm act}$ or $R_{\rm st} < \lvert R\rvert < R_{\rm act}$; After Case III	1	1	0	$P_{\rm L}^{\rm es}$

- Case I: When $\Delta f < f_{\rm dz}$ and $R < R_{\rm dz}$, the system inertia and damping are sufficient, and the FR is not required.
- Case II: When $f_{\rm dz} < |\Delta f| < f_{\rm st}$ and $R_{\rm dz} < |R| < R_{\rm st}$, the system imbalance power caused by disturbance is limited and does not require deep FR. The droop control can ensure frequency stability of system.
- Cases III and IV: When $f_{\rm st} < |\Delta f| < f_{\rm act}$ or $R_{\rm st} < |R| < R_{\rm act}$, the power imbalance is severe, requiring the WTS to release or absorb power urgently. Inertia control is first used by the WTS, along with the power excitation method that evaluates the disturbance. Subsequently, the operation is switched to Case IV to quickly release power.

Considering the aforementioned control stages and system operation cases, a reference implementation of the proposed APC strategy is developed, as shown in Fig. 7.

V. VERIFICATION

In this work, effectiveness and advancement of the proposed APC control strategy are verified by hardware-in-the-loop experiment of a single grid-tied WTS (with reference to Fig. 1) and by MATLAB/Simulink simulation of a standard IEEE 4-machine-2-area (4M2A) system. Main parameters of the experiment system are shown in Table II, where the frequency threshold parameters are chosen in accordance with the requirement of the specific national grid code [18].

TABLE II
MAIN PARAMETERS OF SINGLE WTS MODEL.

Parameter	Value	Parameter	Value
U	380 V	f_{N}	50 Hz
L	4.3 mL	Z	0.01+j1.2 Ω
P	30 kW	Load	36 kW
P_{c}	0.2 kW	U_{dc}	800 V
Small disturbance	2 kW	Large disturbance	6 kW
f_{dz}	0.05 Hz	R_{dz}	0.5 Hz/s
f_{st}	0.1 Hz	R_{st}	1.5 Hz/s
f_{act}	0.5 Hz	R_{act}	2 Hz/s

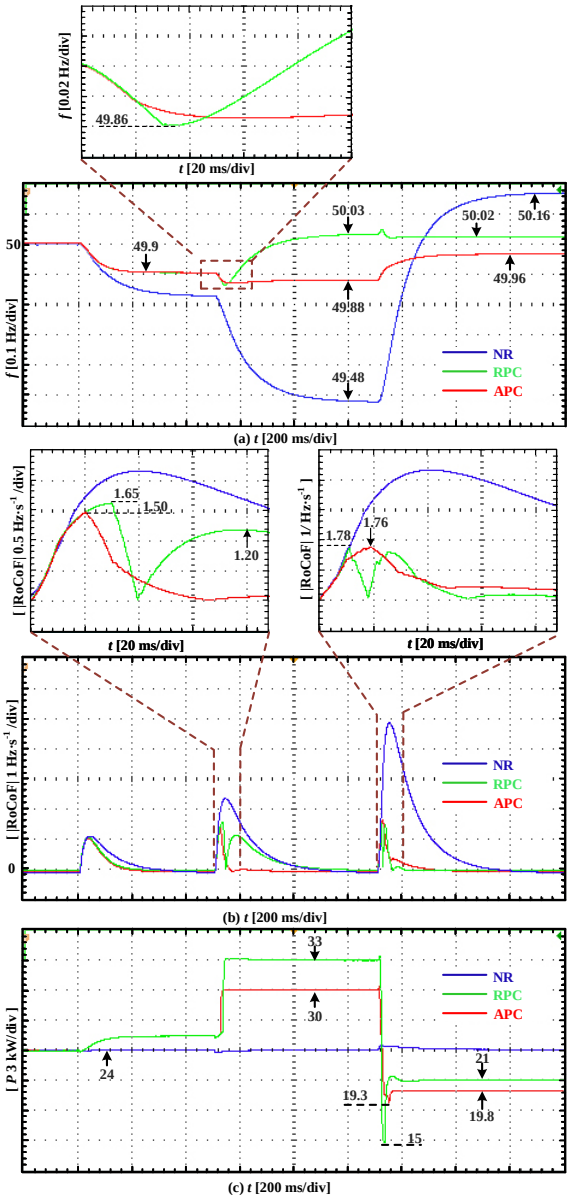

Fig. 8. (a) Frequency, (b) RoCoF, and (c) active power results of single WTS.

A. Verification based on Single Grid-Tied WTS

Three disturbances, encompassing two disturbances in the same direction and a subsequent reverse disturbance, are introduced to the single grid-tied WTS with 40% wind power penetration, and the frequency dynamics are compared in Fig. 8. At 1.5 s, the load power is suddenly increased by 2 kW. The system frequency is reduced to 49.81 Hz without FR strategy, and the frequency-related protection is not triggered. Under the RPC and APC control strategies, since f_{st} and R_{st} are not reached, the WTS operates in droop mode that slightly improves the frequency response; the fast FR service does not activate in this case. At 2 s, the system load power increases by 6 kW, and the natural frequency drops to 49.48 Hz, exceeding f_{act} and triggering the protection. When the RPC control strategy is adopted, the WTS directly outputs the maximum auxiliary power of 9 kW, which corresponds to 0.3 p.u. of its rated power. However, this is larger than the disturbance power, and leads to reversed frequency deviation of system. By adopting the APC control strategy, the disturbance level is estimated first. Then, the WTS quickly participates in FR and counteracts the disturbance, assuring frequency stability and avoiding the secondary frequency disturbance caused by excessive FR.

At 2.6 s, the system load is suddenly reduced by 10 kW, and the frequency deviation is reversed. Without auxiliary FR strategy, the RoCoF will trigger frequency-related protection. When the RPC control strategy is adopted, the power output by WTS is suddenly reduced to 15 kW [see Fig. 8(c)], resulting in secondary fluctuation of RoCoF. Conversely, when the APC control strategy is adopted, the disturbance is estimated and compensated accurately, yet avoiding the secondary disturbance caused by switching from the maximum to minimum power output. Improved performance of frequency indexes is obtained in this case.

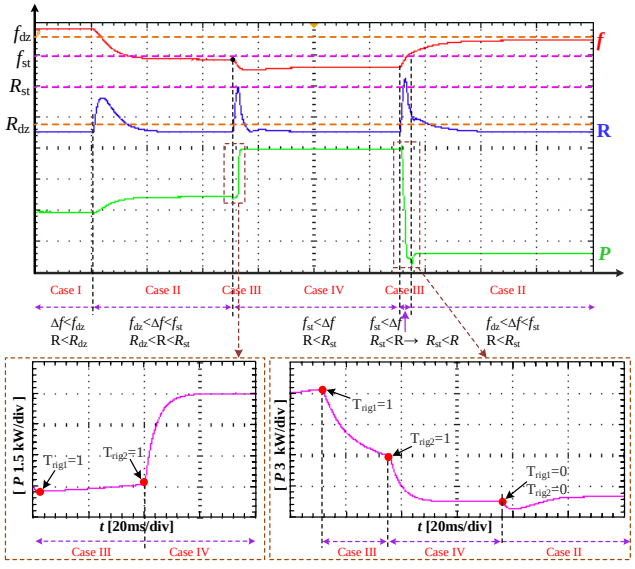

Fig. 9. Case switching process under the APC strategy.

The detailed switching process of APC control strategy is shown in Fig. 9. The system initially operates in steady state (Case I), and T_{rig3} is set to 1. After the small disturbance at 1.5 s, f and RoCoF cross the dead-zone threshold, i.e., $f_{\mathrm{dz}} < |\Delta f| < f_{\mathrm{st}}$ and $R_{\mathrm{dz}} < |R| < R_{\mathrm{st}}$; T_{rig3} is set to 0, triggering the droop control (Case II). At 2 s, the system is disturbed again, and the frequency crosses the limit f_{st},

triggering Case III and T_{rig1} is set to 1. A reverse excitation of 0.2 kW is applied to the system during the disturbance estimation; at the same time, the inertia control is used, ensuring the rapidity and continuity of the FR. The disturbance power is estimated to be 6 kW, which is close to the applied disturbance power in total (8 kW). Subsequently, T_{rig2} is set to 1, and the WTS operation is switched to Case IV for disturbance power compensation. At 2.6 s, the system load power is suddenly reduced, causing a reverse disturbance to system frequency, i.e., $R_{\mathrm{st}} < R$. A positive excitation of 0.2 kW is applied to the system for disturbance estimation, followed by the reduction of WTS output power to 19.3 kW. Finally, when the frequency indexes satisfy $f_{\mathrm{dz}} < f < f_{\mathrm{st}}$ and $R < R_{\mathrm{st}}$, the WTS control is switched to Case II, and the system exits FR smoothly by using droop control.

B. Verification based on 4M2A System

Compared to the standard IEEE 4M2A system, the studied system (see Fig. 10) replaces the 100-MW G4 generator by a WTS. The APC and RPC strategies are compared comprehensively based on simulation results of this system.

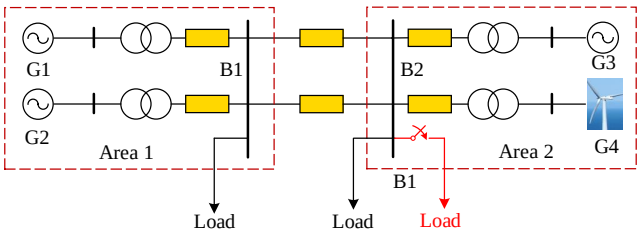

Fig. 10. Diagram of the studied 4M2A multi-machine system.

Fig. 11 demonstrates the frequency dynamics and power output by WTS, when two disturbances are sequentially introduced to the system. When the system load is suddenly increased by 20 MW at 20 s, the natural frequency of system rapidly drops to 49.73 Hz due to the low inertia and weak damping of grid. In addition to the generation power, the RPC control enables the WTS to output the maximum FR power of 28 MW, which is larger than the disturbance power and causes reverse deviation of system frequency. In this case, although the frequency is restored to the normal range after certain time, the surplus power output reduces the economy of grid-tied WTS. Compared to RPC, the proposed strategy firstly estimates the disturbance level, and provides FR power support based on the estimated 13 MW. The system nadir and RoCoF meet the threshold requirements during transient, and the output FR power is closer to disturbance compared to the RPC control.

At 35 s, the system suffers from a larger disturbance when the load power is suddenly increased by 40 MW. In the case of natural frequency response, the frequency nadir becomes 49.44 Hz, which triggers frequency-related protection. APC and RPC strategies provide similar effects in terms of frequency response. At this time, the disturbance estimated by APC (27 MW) is close to the WTS output limit (28 MW, which is also the output by using RPC control).

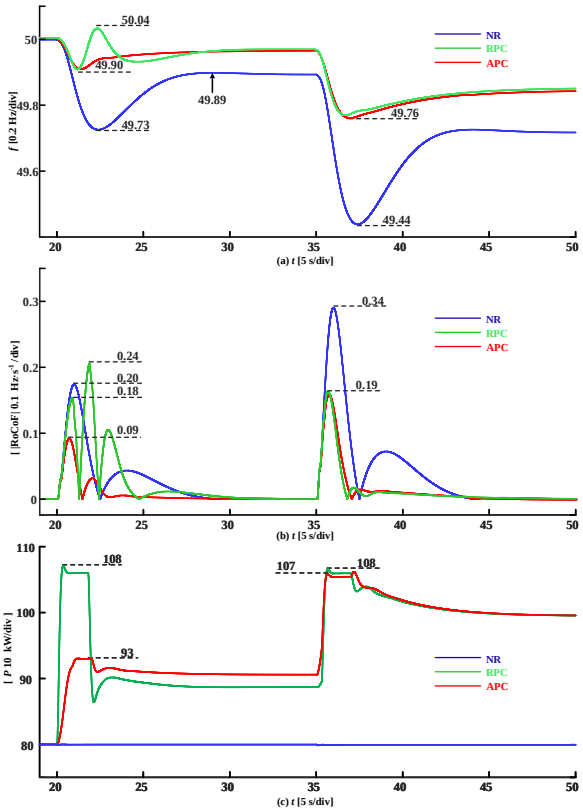

Fig. 11. (a) Frequency, (b) RoCoF, and (c) active power of the 4M2A system.

Simulation results in the 4M2A system again proved the superiority of the proposed strategy, namely, it avoids the blindness of constant compensation according to the maximum power and the secondary disturbance to frequency, realizing accurate FR support by the WTS.

VI. Conclusion

In this paper, an adaptive control strategy of the WTS is developed for better FR support. Through theoretical and simulation analyses, the power excitation method developed in this paper, which makes use of a low power injection at the moment of disturbance, is proved to be feasible for online disturbance estimation. This serves as the foundation of proposed APC. Compared to the RPC control, the proposed strategy enables more effective WTS participation in the system FR based on the estimated disturbance. According to the real-time information of f and RoCoF, the APC strategy accurately switches between different cases, thereby improving the frequency response characteristics of the grid-tied WTS.

References

[1] J. Hu, L. Sun, X. Yuan *et al.*, "Modeling of Type 3 wind turbines with df/dt inertia control for system frequency response study," *IEEE Trans. Power Syst.*, vol. 32, no. 4, pp. 2799–2809, 2017.

[2] L. Xiong, X. Liu, Y. Liu, and F. Zhuo, "Modeling and stability issues of voltage-source converter dominated power systems: A review," *CSEE J. Power Energy Syst.*, to be published, doi: 10.17775/CSEE-JPES.2020.03590.

[3] M. Kheshti, L. Ding, M. Nayeripour *et al.*, "Active power support of wind turbines for grid frequency events using a reliable power reference scheme," *Renew. Energ.*, vol. 139, pp. 1241–1254, 2019.
[4] J. Fang, H. Li, Y. Tang, and F. Blaabjerg, "On the inertia of future more-electronics power systems," *IEEE J. Emerg. Sel. Top. Power Electron.*, vol. 7, no. 4, pp. 2130–2146, 2019.
[5] K. R. Palanisamy and G. Yang, "Future low-inertia power systems: Requirements, issues, and solutions - a review," *Renew. Sust. Energ. Rev.*, vol. 124, pp. 2799–2809, 2020.
[6] F. Teng and G. Strbac, "Assessment of the role and value of frequency response support from wind plants," *IEEE Trans. Sustain. Energ.*, vol. 7, no. 2, pp. 586–595, 2016.
[7] L. Ruttledge and D. Flynn, "Emulated inertial response from wind turbines: Gain scheduling and resource coordination," *IEEE Trans. Power Syst.*, vol. 31, no. 5, pp. 3747–3755, 2016.
[8] A. Attya, J. Dominguez-Garcia, and O. Anaya-Lara, "A review on frequency support provision by wind power plants: Current and future challenges," *Renew. Sust. Energ. Rev.*, vol. 81, pp. 2071–2087, 2018.
[9] F. Díaz-González, M. Hau, A. Sumper, and O. Gomis-Bellmunt, "Participation of wind power plants in system frequency control: Review of grid code requirements and control methods," *Renew. Sust. Energ. Rev.*, vol. 34, pp. 551–564, 2014.
[10] K. Liu, Y. Qu, H. Kim, and H. Song, "Avoiding frequency second dip in power unreserved control during wind power rotational speed recovery," *IEEE Trans. Power Syst.*, vol. 33, no. 3, pp. 3097–3106, 2018.
[11] Z. Chu, U. Markovic, G. Hug, and F. Teng, "Towards optimal system scheduling with synthetic inertia provision from wind turbines," *IEEE Trans. Power Syst.*, vol. 35, no. 5, pp. 4056–4066, 2020.
[12] J. Fang, P. Lin, H. Li *et al.*, "An improved virtual inertia control for three-phase voltage source converters connected to a weak grid," *IEEE Trans. Power Electron.*, vol. 34, no. 9, pp. 8660–8670, 2019.
[13] G. Xu, F. Liu, J. Hu, and T. Bi, "Coordination of wind turbines and synchronous generators for system frequency control," *Renew. Energ.*, vol. 129, pp. 225–236, 2018.
[14] A. Annamraju and S. Nandiraju, "Robust frequency control in a renewable penetrated power system: an adaptive fractional order-fuzzy approach," *Prot. Control Mod. Power Syst.*, vol. 4, p. 1, 2019.
[15] M. Jing, Z. Song, Y. Zhang *et al.*, "Robust stochastic stability analysis method of DFIG integration on power system considering virtual inertia control," *IEEE Trans. Power Syst.*, vol. 32, no. 5, pp. 4069–4079, 2017.
[16] M. Arani and E. El-Saadany, "Implementing virtual inertia in DFIG-based wind power generation," *IEEE Trans. Power Syst.*, vol. 28, no. 2, pp. 1373–1384, 2013.
[17] S. Itani, U. Annakkage, and G. Joos, "Short-term frequency support utilizing inertial response of DFIG wind turbines," in *2011 IEEE Power and Energy Society General Meeting*, 2011, pp. 1–8.
[18] L. Xiong, X. Liu, D. Zhang, and Y. Liu, "Rapid power compensation based frequency response strategy for low inertia power systems," *IEEE J. Emerg. Sel. Top. Power Electron.*, vol. 9, no. 4, pp. 4500–4513, 2021.
[19] L. Xiong, F. Zhuo, F. Wang *et al.*, "Static synchronous generator model: a new perspective to investigate dynamic characteristics and stability issues of grid-connected pwm inverter," *IEEE Trans. Power Electron.*, vol. 31, no. 9, pp. 6264–6280, 2016.
[20] Q. Shi, G. Wang, L. Fu *et al.*, "Virtual inertia control of D-PMSG based on the principle of active disturbance rejection control," *J. Electr. Eng. Technol.*, vol. 10, no. 5, pp. 1969–1982, 2015.
[21] L. Xiong, F. Zhuo, F. Wang *et al.*, "Frequency trajectory planning based strategy for improving frequency stability of droop-controlled inverter based standalone power systems," *IEEE J. Emerg. Sel. Top. Circuits Syst.*, vol. 11, no. 1, pp. 176–187, 2021.

Hongqing Liu received the B.S. degree from the Nanchang University, Nanchang, China, in 2016. He is currently pursuing the master's degree with the School of Electrical and Power Engineering, China University of Mining and Technology, China.

His current research interests include renewable energy generation and stability analysis.

Xiaokang Liu (Member, IEEE) received the double M.Sc. degrees in electrical engineering from Xi'an Jiaotong University, Xi'an, China, and Politecnico di Milano, Milan, Italy, in 2016, and the Ph.D. degree (*summa cum laude*) in electrical engineering from Politecnico di Milano, in 2021.

He is currently an Assistant Professor with the Department of Electronics, Information, and Bioengineering, Politecnico di Milano. His research interests include electromagnetic compatibility, power electronics, and signal integrity.

Dr. Liu was a recipient of the International Union of Radio Science Young Scientist Award, in 2021, and the 2021 Richard B. Schulz Best EMC Transactions Paper Award.

Liansong Xiong (Senior Member, IEEE) received the M.S., and Ph.D. degrees in electrical engineering from Xi'an Jiaotong University (XJTU), Xi'an, China, in 2012 and 2016, respectively.

Since 2014, he has been with the School of E-learning, XJTU, as a part-time *Faculty Member*. In 2016, he joined the School of Automation, Nanjing Institute of Technology (NJIT), Nanjing, China, introduced in High-Level Academic Talent Plan of NJIT. From 2017 to 2019, he joined the Department of Electrical Engineering, The Hong Kong Polytechnic University (PolyU), Hong Kong, as a Research Associate. His current research interests include power quality, multilevel converter, renewable energy generation, and power system stability.

Dr. Xiong is a *Senior Member* of the IEEE and the China Electrotechnical Society, and a member of the China Power Supply Society (CPSS) and the China Society for Electrical Engineering. He has served as the Guest Associate Editor for the Frontiers in Energy Research, the Program Co-Chair of the 3rd Asia Energy and Electrical Engineering Symposium (AEEES 2021), and the Technical Program Committee Member of IEEE Workshop on Wide Bandgap Power Devices and Applications in Asia (WiPDA-Asia 2018). He received the Best Conference Paper Award once in the international conference and the Excellent Paper Award seven times in domestic conferences. He was honored with the First Prize of CPSS Scientific and Technological Progress Award in 2021, the ICPES Young Scientist Award in 2020, the Best Paper Award of Shaanxi Province in 2020, and the Excellent Doctoral Dissertation of XJTU and Shaanxi Province in 2018.

Mingxian Li received the B.S. degree from Tianjin University of Science and Technology, Tianjin, China, in 2017. He has been working toward the master's degree in the School of Electrical and Power Engineering, China University of Mining and Technology, China, in 2021. From 2021, he worked in Jiaxing Power Supply Company of State Grid, Jiaxing, Zhejiang, China.

His current research interests include renewable energy generation and stability analysis.

Yixin Zhu received the B.S., M.S. and Ph.D. degrees in electrical engineering all from Xi'an Jiaotong University, Xi'an China, in 2009, 2011 and 2015, respectively. In 2016, he joined Jiangnan University as a Lecturer. He is currently with the School of IoT engineering, Jiangnan University.

His research interests include the design, control and application of the high-power active power filter, the photovoltaic grid-connected inverter, and also the modeling, analysis and power management of the microgrid.